A Very High Frequency dc-dc Converter Based on a Class Φ_2 Resonant Inverter

Juan M. Rivas[†‡], Olivia Leitermann[‡], Yehui Han[‡], David J. Perreault[‡]
[‡]Laboratory For Electromagnetic And Electronic Systems
Massachusetts Institute Of Technology, Room 10-171
Cambridge, Massachusetts 02139
[†]Ge Global Research
1 Research Circle
Niskayuna, Ny 12309
Email: djperrea@mit.edu

***Abstract*— This paper introduces a new dc-dc converter suitable for operation at very high frequencies under on-off control. The converter power stage is based on a resonant inverter (the Φ_2 inverter) providing low switch voltage stress and fast settling time. A new multi-stage resonant gate driver suited for driving large, high-voltage rf MOSFETS at VHF frequencies is also introduced. Experimental results are presented from a prototype dc-dc converter operating at 30 MHz at input voltages up to 200 V and power levels above 200 W. These results demonstrate the high performance achievable with the proposed design.**

***Index Terms*— resonant dc-dc converter, very high frequency (VHF), class Φ inverter, class phi inverter, class F power amplifier, class E inverter, resonant gate drive, resonant rectifier, harmonic peaking, on-off control, burst-mode control, cycle skipping control.**

I. Introduction

Power density and response speed are important performance metrics in dc-dc power converters. Increases in switching frequency potentially enable improvement of both of these metrics: higher switching frequencies permit the use of smaller-valued (and often physically smaller) passive components having reduced energy storage requirements. Reduced intermediate energy storage, coupled with a shorter switching period, permits more agile response to changes in operating condition. There is thus strong motivation to move to greatly increased switching frequencies if losses, switch driving, control, and other design challenges can be addressed.

Zero-voltage-switching (ZVS) resonant dc-dc converters offer the opportunity to operate at higher frequencies, but pose a number of design challenges. First, designs of this type often suffer from high device voltage stress [1]–[11]. Driving of transistors also becomes a challenge as frequencies are increased, due to both loss considerations and the difficulty of achieving sufficiently fast switching transitions. Moreover, it is often difficult to achieve efficient operation of ZVS resonant converters across a wide load range, owing to resonating losses (for ZVS operation) that do not scale with output power delivery.

This paper introduces a new resonant dc-dc converter and associated driving and control methods that address the above challenges. The converter power stage is based on a resonant inverter (the Φ_2 inverter) that provides low switch voltage stress and fast settling time. The proposed power stage is operated at fixed switching frequency and duty ratio. To achieve output control and high efficiency across a wide load range, we adopt on/off control [8]–[14]. We also introduce a new multi-stage resonant gate drive that provides low-loss driving of high-voltage MOSFETS at VHF frequencies, and is well suited to on/off control. Together, these circuit designs and methods yield extremely high performance.

Section II of the paper introduces the system structure and control approach. Detailed descriptions of the proposed converter and its constituent elements are also presented. The new multi-stage resonant gate drive system is treated in Section III. The results presented throughout this document demonstrate the efficacy of the proposed approach. Finally, Section IV concludes the paper.

II. Proposed Converter System

A. System Structure

Figure 1 shows the general structure of the proposed dc-dc converter. The converter power stage comprises a resonant inverter, a transformation stage, and a resonant rectifier. The resonant inverter accepts a dc input voltage, and generates very high frequency (VHF) ac, which is processed through the transformation stage to produce different ac voltage and current levels. The resonant rectifier then converts the transformed ac power back to dc. A multi-stage resonant gate drive is employed to drive the inverter switch, enabling efficient operation at much higher frequencies than would otherwise be possible.

Regulation of the converter output voltage can be achieved through on/off control of the inverter [8]–[14]. In this approach, the power stage is gated on and off at a modulation frequency that is far lower than the inverter switching frequency. By controlling the fraction of time that the inverter stage runs (and delivers power to the output) the output voltage can be regulated to a desired reference level.

Key advances in the system developed here are in the design of the power stage and the gate drive, and in how

978-1-4244-1668-4/08/$25.00 ©2008 IEEE

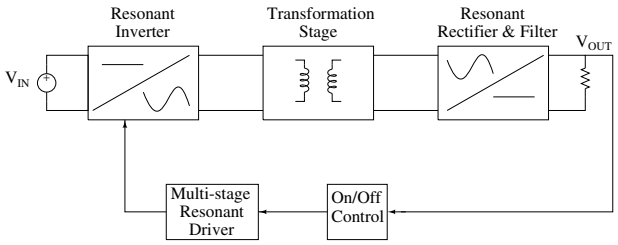

Fig. 1. General structure of the proposed dc-dc converter.

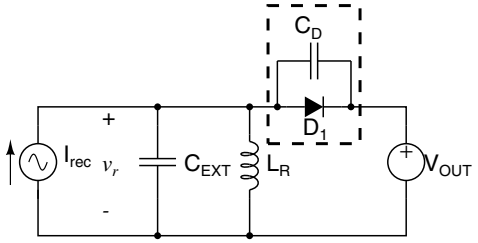

Fig. 3. Resonant rectifier.

these elements are specifically optimized to achieve high performance under on/off control. We focus on each of the subsystems in turn and describe the design procedure of a 200 W dc-dc converter operating at 30 MHz with an input voltage range of‘ 160 V to 200 V and output voltage of 33 V.

B. Rectification and Voltage Transformation

Figure 2 shows the schematic of the Φ_2-based dc-dc converter introduced here. The figure outlines the different stages of the converter corresponding to the general structure shown in Fig. 1. We begin by considering how the rectifier and voltage transformation stages of the converter may be designed. For design purposes, the resonant rectifier can simply be modeled as illustrated in Fig. 3, which shows the resonant rectifier driven from a sinusoidal current source and loaded with a constant voltage at the output. Together, the large energy storage at the output and the on-off scheme regulating the output voltage of the converter allow us to treat the output voltage of the rectifier as constant for design purposes. In the figure, the rectifier is modeled as being driven by a sinusoidal current source of magnitude I_{rec}. The resonant inductor L_R provides a path for the dc current and resonates with the capacitances C_D and C_{EXT} shown in the Figure. C_D represents the diode non-linear capacitance while C_{EXT} accounts for external capacitance added plus the parasitic interwinding capacitance of inductor L_R.

It is possible to describe the voltage-current relationship of a resonant rectifier in terms of an equivalent input impedance in a describing-function sense [9], [15]. In our design the resonant elements were tuned to make the input look nearly resistive at the fundamental frequency (That is, the fundamental of the voltage v_r is in phase with the drive current i_{rec}). Alternatively, if the rectifier is tuned to appear appropriately reactive at the switching frequency, resonance between the interconnect network and the rectifier network can be used to provide voltage gain from the input to the output. The input current amplitude is selected to provide the desired output power. The amplitude and conduction angle of the diode current depend on the component values. By adjusting the net capacitance ($\mathrm{C}_D \| \mathrm{C}_{EXT}$) in parallel with the resonant inductor, we can trade off the length of the conduction interval and the peak reverse voltage across the diode. In some implementations it is convenient to have a conduction angle close to 50 percent, as this provides a good tradeoff between peak diode forward current and reverse voltage. If additional capacitance is required, this can either be added externally or can be solely provided by additional diode area, which can have the added benefit of reducing the overall conduction loss in the rectifier. For the 200 W design presented here we use a pair of silicon carbide Schottky diodes (Cree CSD10030) in parallel[1]. In the design presented here, the corresponding resonant capacitance ($\mathrm{C}_D \| \mathrm{C}_{EXT}$) of Fig. 3 is only provided by the non-linear capacitance of the diodes.

The tuning of the rectifier stage was done numerically in SPICE, which required an accurate diode model. Parameters for the non-linear diode capacitance were obtained by measuring the diode capacitance (C_{KA} =548 pF, 163 pF, and 119 pF , at $\mathrm{f_s}$=1 MHz) at three different bias voltages (V_{KA}=0, 11 V, and 23 V respectively) and solving for V_J and m in the equation: $C_{KA} = C_{j0}/(1 + \frac{v_{KA}}{V_J})^m$. For the CSD10030 diode: C_{j0} = 548.3 pF, V_J = 0.78 V, and m=0.45 for $0 \leq v_{KA} < 100$ V. The CSD10030 datasheet indicates that for $v_{KA} > 100$ V the diode capacitance is approximately constant (C_{KA} = 62.6 pF). In addition to the capacitance, the SPICE model of the diode incorporates 6 nH of lead inductance (between lead and the back of the TO-220 package), and 0.15 Ω of equivalent series resistance. The forward characteristic of each diode is modeled as a constant forward drop ($\mathrm{V_{d,ON}}$=507 mV) in series with a resistor ($\mathrm{R_S}$=89.7 mΩ). With the appropriate model of the diodes, we proceeded to iteratively adjust the value of L_R and I_{rec} in SPICE and look for the values at which the fundamental of v_r and i_{rec} were in phase, and for which the rectifier delivered sufficient output power.

Figure 4 (a) shows a SPICE simulation of the rectifier shown in Fig. 3, tuned to appear resistive at the fundamental frequency. For the conditions shown in the figure, $\mathrm{L_R}$=75 nH, f_s = 30 MHz and $|I_{rec}|$= 7.15 A. The output power P_{OUT} delivered to the 33 V load is 200 W. Figure 4 (b) shows the sinusoidal input current, and the fundamental component of the input voltage, from which the an equivalent resistance of approximately 8.4 Ω can be extracted.

Generally, the equivalent rectifier resistance will not correspond to the load resistance value at which a given power will be delivered by the Φ_2 inverter with greatest efficiency. Hence, there is a need to provide some sort of impedance transformation between the inverter and rectifier (e.g., by using a matching network [16], [17] and/or a transformer). For the dc-dc converter design presented here, a 4 to 1 impedance transformation is realized using a 1:1 autotransformer, with the transformer parasitics absorbed into the resonant tank of the inverter and the rectifier network. As will be discussed

[1]These devices have a positive forward conduction thermal coefficient, which allows the paralleling of multiple devices.

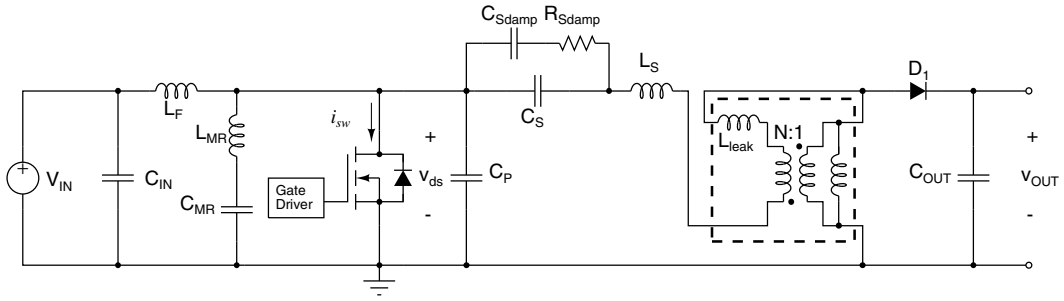

Fig. 2. Dc-dc converter as implemented with an autotransformer.

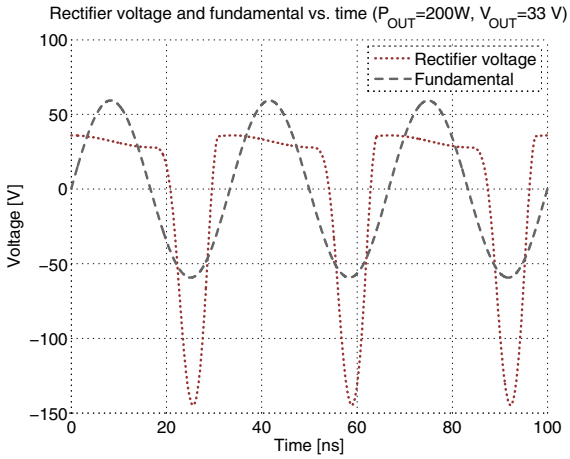

(a)

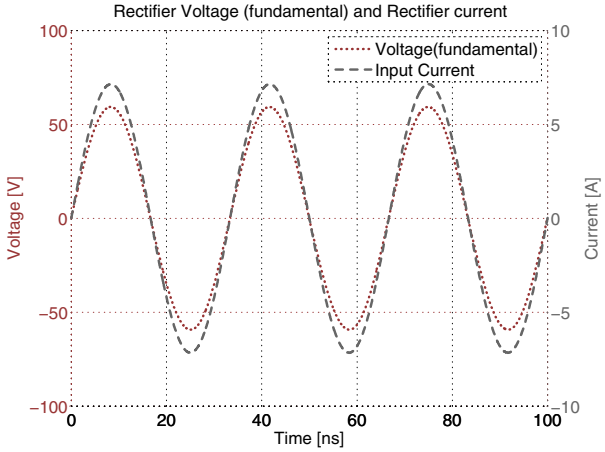

(b)

Fig. 4. (a) Rectifier voltage and its fundamental component. (b) Fundamental component of the input voltage and input current. $P_{OUT} = 200$ W. $f_s =$ 30 MHz, L_R=75 nH, Q_L=160. The equivalent resistance of the rectifier under this condition is 8.4 Ω.

in subsequent sections, the optimal value for the equivalent resistance for the rectifier as seen at the input of the autotransformer is a trade off between the resonating currents circulating within the inverter and the maximum power that can be delivered.

Notice that in the schematic of Fig. 2 the magnetizing inductance of the autotransformer functions as the rectifier's resonant inductance (L_R in Fig. 3). Designing an autotransformer

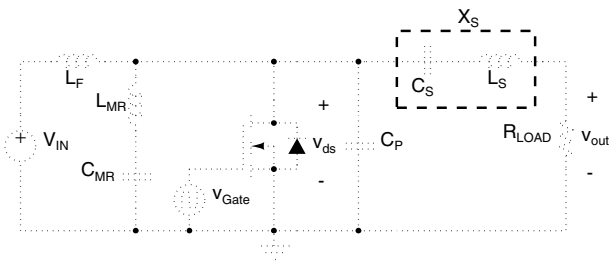

Fig. 5. The Φ_2 resonant inverter.

with a coupling coefficient close to unity is desirable in order to achieve an accurate 4 to 1 impedance transformation, but this may be hard to achieve in practice. An inspection of Fig. 2 will show, the autotransformer leakage inductance L_{leak} can be absorbed by the inverter's inductor L_S. Although parasitic capacitance between the autotransformer windings and the converter ground can be absorbed by the rectifier capacitances, care should be taken to minimize parasitic capacitances across the windings.

C. Φ_2 Resonant Inverter Design

When operating at very high frequencies, it becomes difficult to implement gate drives for switching elements having floating sources (owing to capacitive currents) so designs having switches with their control ports referenced to constant potentials are often preferred. Likewise, it is often preferable to design inverters using only one semiconductor switch because of the difficulty of accurately commutating among multiple devices in this frequency range. Furthermore, switching high voltage at very high frequencies requires designs that realize zero-voltage-switching (ZVS) to minimize switching losses. Finally, inverters that absorb switch parasitic capacitance and are tolerant of relatively slow gating waveforms are advantageous.

Unfortunately, many inverter designs that meet the above requirements suffer from extremely high voltage stress. For example, the widely-used class E inverter [18], [19] meets all of these requirements, but results in voltage stresses across the switch that can reach over four times the input voltage [20] when the nonlinear capacitance of the device is considered. Other limitations of many inverter topologies appropriate to VHF operation include the use of bulk "rf choke" inductors (which is disadvantageous for rapid transient response and on-

off control), and a tight tie between device parasitic capacitance and achievable output power and frequency [10], [13].

In this paper we use a recently-developed single-switch ZVS inverter topology that overcomes the limitations described above. The so-called Φ_2 inverter (shown in Fig. 5) introduced in [14], [21], [22] is a highly simplified variant of the class Φ inverter [23]–[25]. It operates with a much reduced voltage stress across the switch (slightly over twice the input voltage) and breaks the tight link between semiconductor capacitance, output power, and frequency found in many high frequency resonant designs. Furthermore, the Φ_2 inverter only uses resonant elements (no input choke inductor) thus reducing the energy storage requirements of the converter and providing an inherently faster response. The benefits of this are twofold: it allows a reduction in the overall size of the converter (by reducing input and output bulk capacitance requirements), and improves the control bandwidth.

As introduced in [21], [26], the resonant components of the Φ_2 inverter are selected to achieve shaping of the switch drain voltage into a trapezoidal waveform by controlling the impedance characteristics at the switch drain. Specifically, the design procedure detailed there calls for certain characteristics in the magnitude and phase of the impedance seen looking into the drain to source port of the MOSFET during its off state. Specifically, the design procedure requires:

- The impedance at the fundamental switching frequency is 30°-60° inductive.
- The impedance at the second harmonic is small due to the series resonance between L_{MR} and C_{MR}.
- The impedance at the third harmonic is capacitive in phase and its magnitude is several dB (between 4 and 8) below the impedance magnitude at the fundamental.
- The values of X_S and R_{LOAD} are selected to achieve the desired power transfer based on the voltage division from the trapezoidal operating waveforms of the inverter.

The inverter design starts by obtaining values for components L_S and C_S forming the reactance X_S in Fig. 5. Here, X_S was designed to look inductive at the fundamental frequency (30 MHz). Assuming the drain to source voltage of the MOSFET resembles a trapezoid going from zero to an amplitude of twice the input voltage, we can determine the value of inductor L_S by assuming all power will be delivered at the fundamental frequency. Moreover, we know that R_{LOAD}=33 Ω in Fig. 5 (the equivalent resistance, at the fundamental, of the rectifier as seen at the input of the autotransformer: $4 \times 8.2\ \Omega$). By solving the equation of the reactive voltage divider formed by the series combination of L_S and R_{LOAD} with a fundamental voltage at the drain node of $\approx \frac{4}{\pi} V_{IN}$ (by further approximating the drain to source trapezoid as a square wave) we find that with L_S=256 nH we can deliver approximately 200 W when V_{IN}=160 V. In practice, the output power of the inverter will be somewhat smaller than predicted because of the lower amplitude of fundamental component of the trapezoidal waveform at the drain node. Here, capacitor C_S=4 nF and only provides dc blocking and presents a relatively low impedance at 30 MHz.

We then proceed to find values for resonant components L_{MR}, C_{MR}, L_F, C_P following the guidelines outlined in [21], [26]. As described in the references, starting values of these components can be found using $L_{MR}=1/15\pi^2 f^2{}_s C_F$, $C_{MR}=15C_F/16$, and $L_F=1/9\pi^2 f^2{}_s C_F$, where $C_F$is a fraction of the total capacitance formed by the switch capacitance and the external capacitance C_P. To minimize conduction losses in the resonant components of the inverter, it is desirable to have relatively high impedance levels at the fundamental and third harmonic while allowing for realizable inductor and capacitor values.

Starting with C_F=20 pF (less than half the $C_{ds} = 55.47$ pF of the ARF521 MOSFET when V_{IN}=160 V) we find L_{MR}=375 nH, C_{MR}=18.75 pF, L_F=625 nH, as starting values for the resonant components of the inverter. The resonant element $L_F$has to be further adjusted to a value of 345 nH and an external capacitance C_P =30 pF has to be added to the drain node (making the total drain to source capacitance equal to 88.5 pF when V_{IN}=160 V) to achieve the impedance characteristics at the fundamental, second and third harmonic of the switching frequency that will result in a trapezoidal $v_{ds}(t)$ waveform with zero-voltage switching and with zero dv/dt at switch turn on. A bode plot of the Φ_2 inverter drain to source impedance $Z_{DS}(f)$ is shown in Fig. 6(a) when the inverter is loaded with the equivalent rectifier resistance. Here,
$\mid Z_{DS} \mid$= 37.5 dBΩ and $\angle Z_{DS}$=40° at the fundamental frequency (30 MHz). Moreover, the impedance magnitude at the fundamental is 7 dB above the impedance at the third harmonic. Notice the notch at 60 MHz. Figure 6(b) shows a transient simulation of the drain to source voltage for the same parameters. Under these conditions the load power is P_{Rload}=174 W when V_{IN}=160 V and P_{Rload}=277 W when V_{IN}=200 V.

D. Dc-dc Converter Implementation

It should now be clear that implementation of the proposed Φ_2-based dc-dc converter requires careful design and placement of the various resonant elements which are tuned to achieve precise waveform characteristics. The authors found it convenient to characterize each element's impedance as it was placed on the PCB prototype board and then measure the impedance at the drain-source port. During the tuning process, the component values in the simulation were continually updated to maintain good agreement between the measured values on the prototype and the simulation. This step was made to verify and account for as many parasitics as was deemed possible.

The non-linear dependency with voltage of both the MOSFET and diode capacitances required impedance measurements throughout the tuning process having both semiconductors properly biased at their respective operating voltages (V_{DS}=160 V for the MOSFET and V_{KA}=33 V). A 250 V 10 μF ceramic capacitor was placed between the measurement device (Agilent 4395 Impedance Analyzer) and the drain node of the converter to protect the analyzer from potentially destructive voltages. The introduction of the blocking capacitor contributed 6 nH of series inductance between the impedance analyzer and the drain node that had to be accounted in our

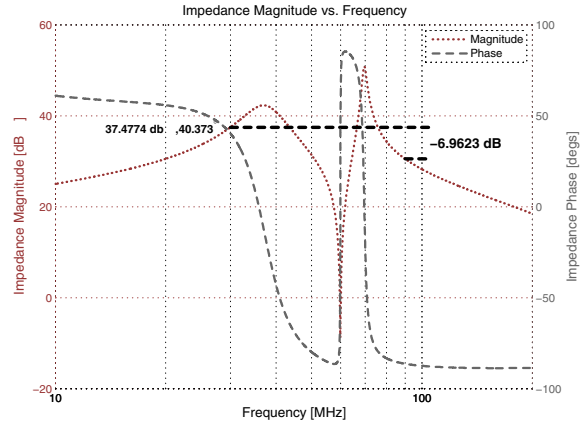

(a) $Z_{DS}(f)$

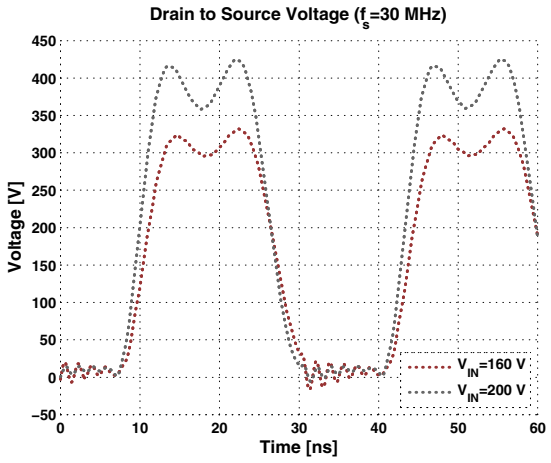

(b) $v_{ds}(t)$

Fig. 6. (a) Drain to Source impedance of the Φ_2 inverter design. Here L_F=345 nH, L_{MR}=375 nH, C_{MR}=18.75 pF, C_P=30 pF, C_S=4 nF, L_S=256 nH, and $R_{LOAD} = 33\ \Omega$. At the fundamental, $\mid Z_{DS} \mid = 37.5\text{dB}\Omega$ and $\angle Z_{DS} = 40°$. The impedance magnitude at the fundamental is 7 dB above the impedance at the third harmonic. Notice the notch at 60 MHz. (b) Drain to source voltage of the Φ_2 Inverter when V_{IN}=160 V and 200 V (Transient Simulation). The waveform shows the drain node achieves ZVS and approximately zero dv/dt at switch turn-on. The simulation accounts for the non-linear capacitance behavior of the ARF521 and of relevant parasitics.

The implementation of the prototype started with placement of the elements forming the rectifier described in Section II-B. The auto-transformer was built on a Teflon rod (9/16 in. diameter, with 12 turns/in threads). The primary winding consists of 3 turns of AWG16 magnet wire, while the secondary has 2 turns. The secondary winding was placed on top of the primary to maximize coupling. Parameter extraction was performed by standard short-and-open-circuit impedance measurements. These measurements were made with the auto-transformer placed on the PCB to account for board parasitic inductances. We used a cantilever model for the transformer as illustrated in Fig. 2. The measured value of L_{leak}=84.8 nH, Lμ=78.5 nH, and the effective turns ratio is N=0.83. The leakage L_{leak} contributes part of the 257 nH needed by the inverter's reactive interconnect X_S.

The reader should keep in mind the resistive behavior of the rectifier is a modeling strategy valid only when the rectifier is in operation. During construction of the prototype, impedance measurements were done under small signal conditions. This means the impedance looking into the auto-transformer and towards the rectifier will not look resistive but will exhibit the parallel resonance formed by L_μ and the diode capacitance under bias.

We proceeded to place the inverter's components on the board, starting with C_{MR} and L_{MR}. These elements are responsible for introducing a null at the second harmonic of the switching frequency. L_{MR} was constructed by winding 9 turns of AWG16 magnet wire on a $3/8$ in. diameter Teflon rod (with 14 turns/in threads). C_{MR} was implemented by connecting 3 (two 56 pF and one 39 pF) porcelain capacitors in series. A measurement of drain impedance placed the resonant frequency of the L_{MR}-C_{MR} combination at 61 MHz. We then put the ARF521 MOSFET in place and continued by adding L_S (with a value of 175 nH that when adding L_{leak} of the autotransformer makes the total value of the branch inductance 259 nH). The last component to be placed was L_F. The designed value of L_F had to be slightly adjusted to precisely achieve ZVS and zero dv/dt in simulation. L_F was made of 9 turns of AWG 16 wire on a $3/8$ in. diam. Teflon rod (14 turns/in. threads) with an off-board value of 384 nH.

With all the components in place, we measured the impedance looking into the drain port. Figure 7(a) shows the measured $Z_{DS}(f)$ and compares it with a SPICE simulation in which the parameters were extracted from measurements on the PCB when V_{IN}=160 V and V_{OUT}=33 V. Figure 7(b) shows the $v_{ds}(t)$ of a transient simulation of the expected behavior dc-dc converter operating at both extremes of the input voltage range. Table I shows measured values of the components in the prototype.

E. Experimental Performance of the Φ_2 dc-dc Converter

Figure 8 displays a photograph of the prototype power stage. Details of the mounting and cooling of the power stage may be found in [22].

To evaluate and measure the steady state performance of the converter, a 33 V dc load was constructed by paralleling 14 50-W Zener diodes (NTE5269A).

To test the power stage of the converter prior to development of a complete gate drive, the gate was driven from a 50 Ω power amplifier. In order to reduce the impact of the 50 Ω output impedance of the power amplifier (Amplifier Research 150A100B) used, a 4:1 (in impedance) bifilar RF transformer (Pulse Engineering p/n CX2024) was connected as a transmission-line transformer (autotransformer) to the input of the gate drive.

Figure 9 shows the drain voltage $v_{ds}(t)$ and the gate voltage $v_{gs}(t)$ of the MOSFET when V_{IN}=160 V. The desired trapezoidal drain waveforms with ZVS switching is achieved (c.f. 6(b)). The drain-gate capacitance C_{rss} is responsible for the distortion in the gate waveform. This issue is addressed by the improved gate driver described in the following section.

Experimental measurements of $v_{ds}(t)$ over the entire operating input voltage range (160 V to 200 V), portrayed in Fig. 10, demonstrate that the peak voltage across the power MOSFET is at most 2.35 times the input voltage.

TABLE I
LIST OF COMPONENTS FOR THE 30 MHZ, 160 V TO 200 V INPUT 33 V OUTPUT Φ_2 PROTOTYPE DC-DC CONVERTER.

Part	Measured Value	Q	Part number
C_{IN}	4 μF (250 V Ceramic)		4x CKG57NX7R2E105M
L_F	384 nH (off-board measurement)	197	9 turns of AWG 16 wire on a $3/8$ in. diam. Teflon® rod with 14 turns/in. threads
MOSFET	ARF521		APT Inc.
L_{MR}	414 nH	185	9 turns AWG 16 wire on a $3/8$ in. diam. Teflon® rod with 14 turns/in. threads
C_{MR}	16.3 pF (porcelain)	10 K 10 K	2x56 pF ATC100B560JW 1x39 pF ATC100B390JW
C_P C_S	28 pF 4 nF	 3 K	Parasitic drain capacitance 4x1 nF MC22FD102J-F
C_{Sdamp}	10 nF		15 nF C3225C0G2E153J
R_{Sdamp}	10 Ω		(SMD1012) ERJ-S14F10R0U
L_S	175 nH	195	5 turns AWG 16 wire on a $3/8$ in. diam. Teflon® rod with 14 turns/in. threads
Auto-transformer	N=0.83 L_{LEAK}=84.8 nH L_μ=78.5 nH		Primary: 2 turns AWG 16 wire Secondary: 3 turns AWG 16 wire on a $9/16$ in. diam. Teflon® rod with 12 turns/in. threads
Diode	2x CSD10030		Cree Inc.
C_{OUT}	4 μF (250 V Ceramic)		4x CKG57NX7R2E105M

TABLE II
SUMMARY OF GATE DRIVE PERFORMANCE REQUIREMENTS.

Attribute	Value
Switching Time	$<< 33ns; \approx 1ns$
Threshold Voltage	$\approx 2.5V$
Target On-state Gate Voltage	$8V$
Gate Voltage Limits	$+/-30V$
Target Duty Cycle	0.3

The output power and the drain efficiency of the converter is presented in Fig. 11 over the input voltage range. The figure demonstrates that the Φ_2 dc-dc converter can achieve high drain efficiency over the entire input range (82.5% to 87.5%).

III. MULTI-STAGE RESONANT GATE DRIVE

In very high frequency power conversion, driving the switching device(s) fast enough and hard enough is a significant challenge. For example, the large gate capacitances of high-power vertical MOSFETS require high currents to switch fast enough. Further complicating the drive is the substantial feedback from the drain voltage through the gate-drain capacitance, especially in high-voltage designs. Additionally, the nonlinearities of all the device capacitances constrain the design of the gate drive. Finally, all these problems must be solved while driving the gate with a total power which is small compared to the output power in order to keep efficiency high.

The specific targets for the prototype device and power converter are summarized in Table II.

The majority of standard gate drive techniques are not well-suited to this problem. For example, the power dissipation of a commercial hard-switched rf driver such as the IXYS DEIC420 is prohibitively large ($> 50W$) for a 200 W dc-dc converter [27]. While resonant gate drives are attractive at these frequencies, a single-stage resonant drive such as those in [8]–[10], [13], [14] would be difficult to realize. In many fields, including RF amplifiers and digital drives, the use of multistage amplifiers or drives is a standard technique to deliver additional power gain, and it is useful for to achieving the current gain necessary here. Thus, a multistage gate drive was implemented here.

In this driver, a small, hard-switching tapered inverter (the "hard-switching inverter") drives a larger resonant inverter (the "resonant drive inverter"), which in turn drives the gate of the main inverter switch via a matching network. Schematics for the hard-switching inverter are shown in Fig. 12, while schematics for the resonant drive inverter are shown in Fig. 13. As will be shown, this structure is suitable for efficiently developing the required drive waveforms.

Use of a hard-switched inverter as a first driver stage is attractive because the resonant drive inverter it feeds operates at substantially lower voltage and power levels and has much smaller capacitances than the main resonant inverter. As illustrated in Fig. 12, the first stage drive includes a 30 MHz clock signal feeding a single CMOS gate whose output is modulated by an enable signal (providing a means for on-off control). This single gate in turn drives a stack of eight CMOS inverters in parallel, providing a tapered drive.

The CMOS hard-switched inverter drives the gate of the resonant drive inverter (Fig. 13), which is a second-harmonic class E inverter [28]. The second harmonic class E inverter is well suited to the gate drive problem. The inverter contains only resonant components and requires no bulk inductor. This provides fast transient response, which is necessary for fast startup and shutdown of the gate drive under on-off control. The second harmonic class E topology is also well-suited to driving low impedances, which is helpful given the low gate impedance to be driven.

To further provide good matching to the very low gate (load) impedance, an L-section matching network was used. This

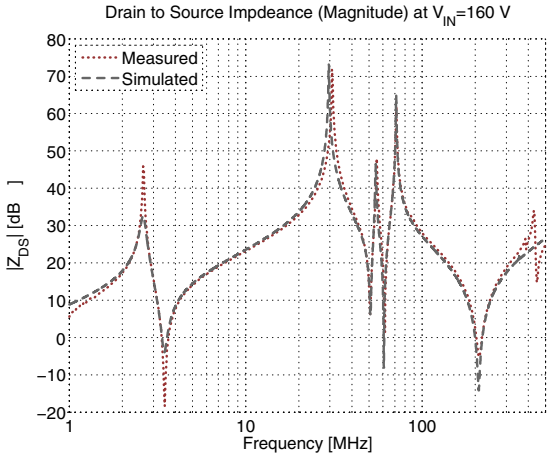

(a) $Z_{DS}(f)$

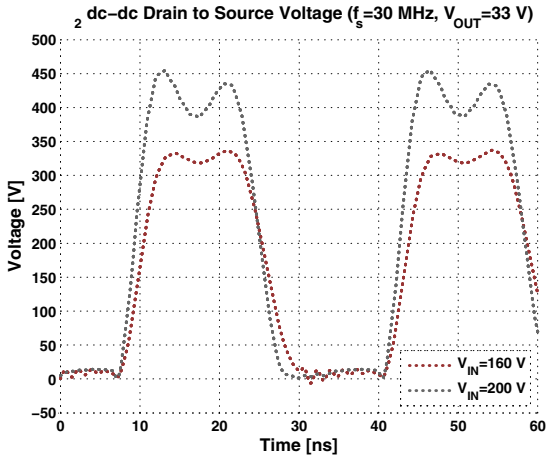

(b) $v_{ds}(t)$

Fig. 7. (a) Comparison between measured and simulated drain to source impedance of the Φ_2 dc-dc converter prototype when V_{IN}=160 V and V_{OUT}=33 V. The differences between this and the plot shown in Fig. 6(a) are explained by accounting for the small-signal impedance of the resonant rectifier (biased to 33 V) during prototype implementation. (b) Drain to source voltage of the Φ_2 dc-dc converter when V_{IN}=160 V and 200 V (Transient Simulation). The waveforms shows almost identical dynamic behavior to the simulated drain to source voltage waveforms of the inverter shown in Fig. 6.

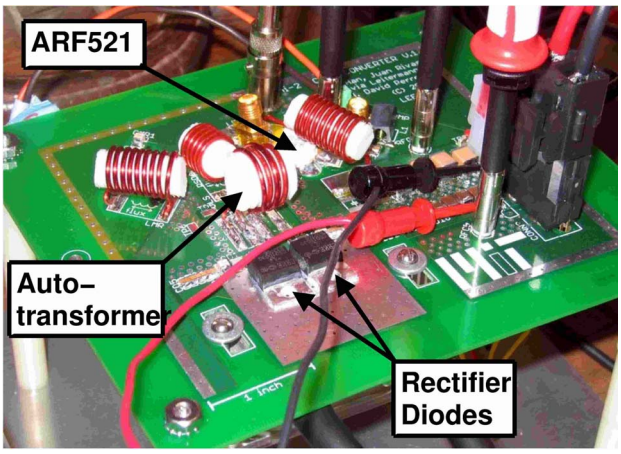

Fig. 8. Prototype Φ_2 dc-dc Converter.

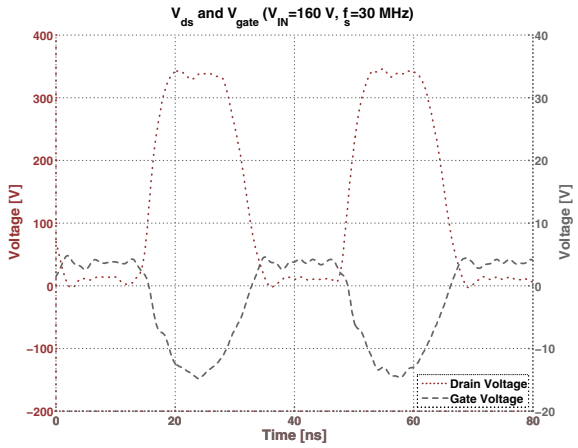

Fig. 9. Experimental MOSFET drain to source and gate voltage at V_{IN}=160 V. The gate is driven from a 50Ω power amplifier through a CX2024 transmission-line transformer.

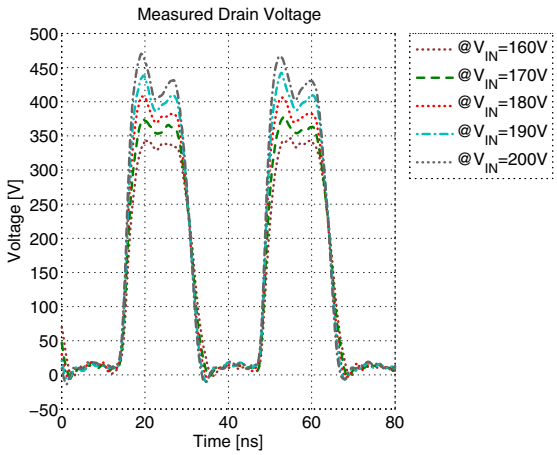

Fig. 10. Experimental drain-to-source voltage v_{ds} for 160 V$\leq$ V_{IN} $\leq$200 V. The peak drain voltage to input voltage ratio is $\simeq$2.35.

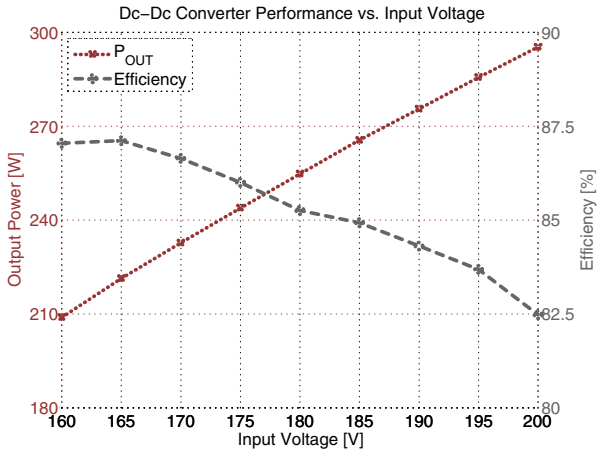

Fig. 11. Experimental output power and drain efficiency vs. input voltage for the prototype dc-dc converter driven with the power amplifier.

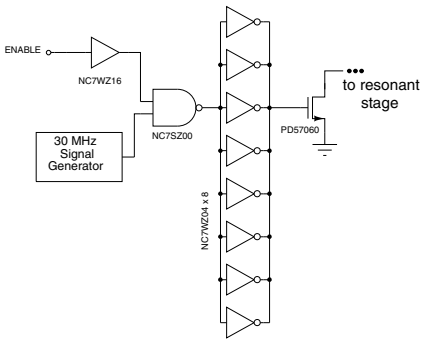

Fig. 12. Auxiliary hard-switched driver.

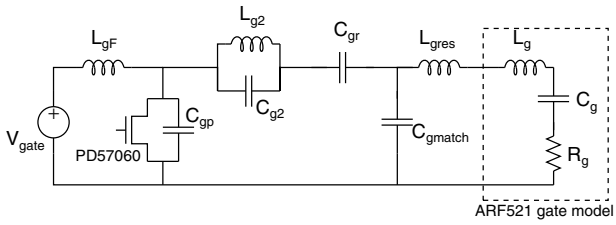

Fig. 13. Resonant second harmonic class E gate driver.

serves to raise the effective load resistance seen by the inverter, thereby reducing resonant losses and improving the sizing of resonant component values in the inverter. Because a dc-pass L-matching network is used, the resonant tank inductance is in series with both the matching inductance and the parasitic gate inductance, enabling these resonant components to be lumped together in one physical inductor which absorbs the parasitic gate inductance. Moreover, this structure allows a dc bias V_{bias} (not shown) to be applied to the gate in order to control switch duty cycle.

Table III contains the values and part numbers of the parts used. The total power dissipation of the gate drive was approximately 3.3 W when the drive was running and approximately 1.3 W static power when the drive was powered but not running. This amounts to less than 2% of the total output power.

Figure 14 shows the output of the hard-switched first stage and the drain waveforms of the auxiliary second harmonic class E gate drive inverter. Note that the second harmonic class E waveforms look like standard class E drain waveforms, switching at approximately zero voltage and zero $\frac{dv}{dt}$.

The gate and drain waveforms of the power stage are shown in Fig. 15. As can be seen from the low drain voltage during on state, the switch is fully enhanced. Note the rapid switching times and the substantial gate voltage in the middle of the on state. Figure 16 compares the performance of the system, in terms of total efficiency and output power, running with the gate drive as described here. A photograph of the gate drive board mounted on the converter is included as Fig. 17.

An advantage of this gate drive design is the speed with which the entire system may be turned on or off. As can be seen in Fig. 18, the full system is approximately in steady state within about 500-1000 ns after an enable command. Since there is very little stored energy, the turn-off is very

TABLE III
COMPONENTS USED IN GATE DRIVE

Device	Manufacturer	Part No.
NAND Gate	Fairchild	NC7SZ00M
Hard-switching Inverters	Fairchild	NC7WZ04
Auxiliary Switch	ST Micro	PD57060

Component	Value	Part No.
L_{gF}	68 nH	1812SMS-68N
L_{g2}	16 nH	2508-16NJL
C_{g2}	417 pF	GRM1885C2A391JA01D + GRM1885C2A270JA01D
C_{gr}	220 pF	C1608C0G2A221J
L_{gres}	30 nH	Custom 1812SMS-33N
C_{gmatch}	3 x 1 nF	3 x ATC100B102KW

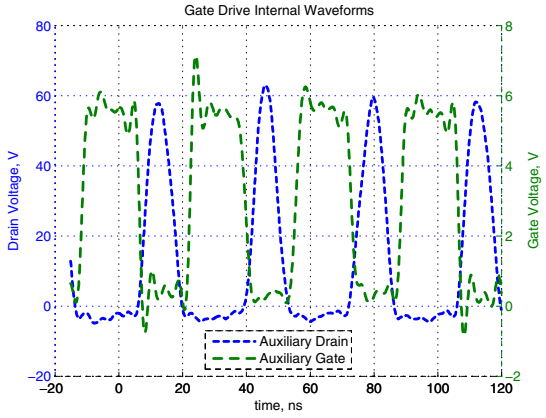

Fig. 14. Experimental internal gate drive waveforms. $V_{IN} = 180V, V_{bias} = -3V$.

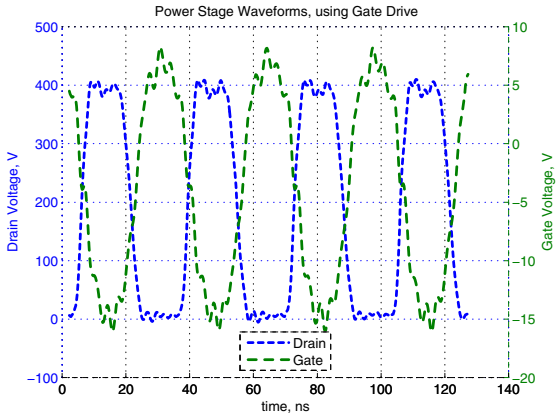

Fig. 15. Experimental power stage waveforms using multistage resonant gate driver. $V_{IN} = 180V, V_{bias} = -3.75V$.

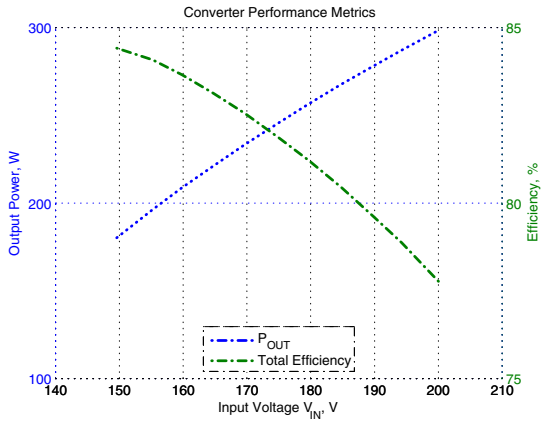

Fig. 16. Experimental performance of the dc-dc converter as measured using the described gate drive. $V_{bias} = -3.75\ V$.

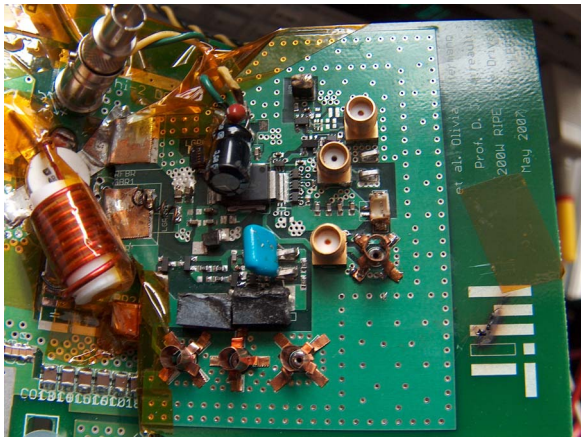

Fig. 17. Photograph of the gate drive board.

rapid as well. Figure 19 shows the turn-off transient. Note that the drain voltage is substantially decayed within 500 ns after disable and that only small oscillations remain beyond 1 μs. This response speed is certainly adequate to implement on-off control as described in [8]–[14].

IV. Conclusion

The dc-dc converter presented here offers significant advantages over previous VHF designs. The power stage, based on the Φ_2 inverter, provides efficient dc-dc conversion at very high frequencies, with few small-valued passive components and low device stresses. The multi-stage resonant gate driver developed here provides high-speed, low-loss driving of the inverter. Due to the small values and energy storage of the passive components in both the power stage and gate driver, the transient response can be very fast compared to conventional designs, and the converter is especially well suited to on-off control. Experimental results from a prototype design operating at 30 MHz and over 200 W at up to 200 V input demonstrate the effectiveness of the proposed design approach.

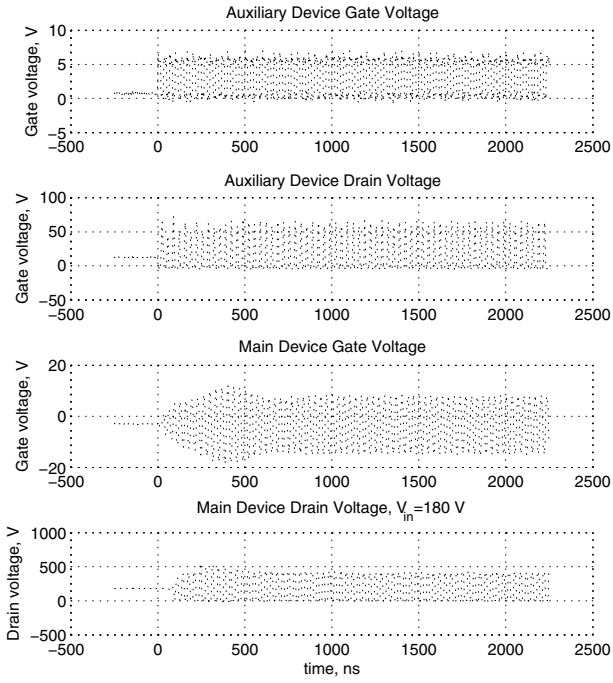

Fig. 18. Experimental turn-on transient with gate drive. $V_{IN} = 180V, V_{bias} = -3V$, load at or above 31 V.

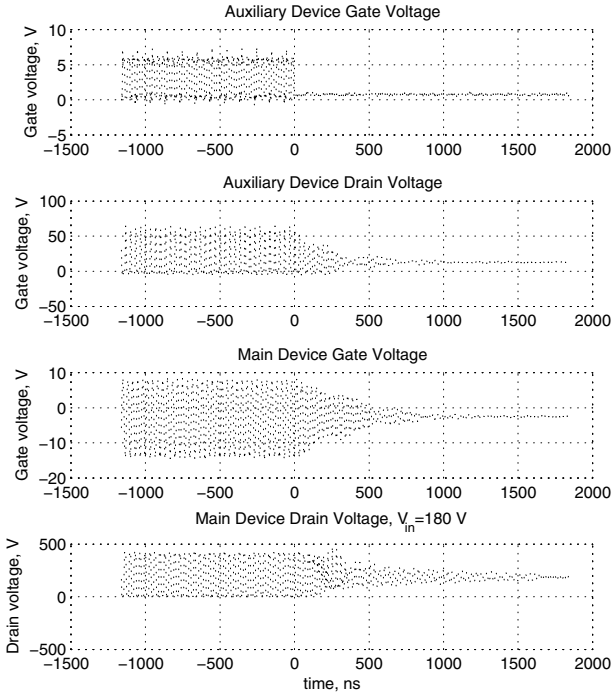

Fig. 19. Experimental turn-off transient with gate drive. $V_{IN} = 180V, V_{bias} = -3V$.

REFERENCES

[1] W. Bowman, J. Balicki, F. Dickens, R. Honeycutt, W. Nitz, W. Strauss, W. Suiter, and N. Zeisse, "A resonant dc-to-dc converter operating at 22 megahertz," in *Third Annual Applied Power Electronics Conference Proceedings*, pp. 3–11, 1988.

[2] R. Gutmann, "Application of RF circuit design principles to distributed power converters," *IEEE Transactions on Industrial Electronics and Control Instrumentation*, vol. IEC127, no. 3, pp. 156–164, 1980.

[3] J. Jóźwik and M. Kazimierczuk, "Analysis and design of class E^2 dc/dc converter," *IEEE Transactions on Industrial Electronics*, vol. 37, no. 2, pp. 173–183, 1990.

[4] H. Koizumi, M. Iwadare, and S. Mori, "Class E^2 dc-dc converter with second harmonic resonant class E inverter and class E rectifier," in *Third Annual Applied Power Electronics Conference Proceedings*, pp. 1012–1018, 1994.

[5] F. Lee, "High-frequency quasi-resonant converter technologies," in *Proceedings of the IEEE*, vol. 76, pp. 377–390, April 1988.

[6] R. Redl, B. Molnar, and N. Sokal, "Class E resonant regulated dc/dc power converters: Analysis of operations and experimental results at 1.5 MHz," *IEEE Transactions on Power Electronics*, vol. PE-1, no. 2, pp. 111–120, April 1986.

[7] R. Redl and N. Sokal, "A new Class-E DC/DC converter family with reduced parts count: Derivation,Topologies, and Design Considerations," in *Technical Papers of the Fourth International High Frequency Power Conversion 1989 Conference*, (Naples, FL), pp. 395–415, May 1989.

[8] J. Rivas, R. Wahby, J. Shafran, and D. Perreault, "New architectures for radio-frequency DC/DC power conversion," in *Power Electronics Specialists Conference, 2004. PESC 04. 2004 IEEE 35th Annual*, vol. 5, pp. 4074–4084Vol.5, 20-25 June 2004.

[9] J. M. Rivas, D. J. Jackson, O. Leitermann, A. D. Sagneri, Y. Han, and D. J. Perreault, "Design Consideration for Very High Frequency dc-dc Converters," in *37^{th} Annual Power Electronics Specialists Conference Proceedings*, pp. 2287–2297, June 2006.

[10] J. M. Rivas, R. S. Wahby, J. S. Shafran, and D. J. Perreault, "New Architectures for Radio-Frequency dc-dc Power Conversion," *IEEE Transactions on Power Electronics*, vol. 21, pp. 380–393, March 2006.

[11] W. A. Tabisz and F. C. Lee, "Zero-Voltage-Switching Multiresonant technique–a novel approach to improve performance of high-frequency quasi-resonant converters," *IEEE Transactions on Power Electronics*, vol. 4, no. 4, pp. 450–458, October 1989.

[12] Y. Lee and Y. Cheng, "A 580 khz switching regulator using on-off control," *Journal of the Institution of Electronic and Radio Engineers*, vol. 57, no. 5, pp. 221–226, September/October 1987.

[13] J. R. Warren, III, K. A. Rosowski, and D. J. Perreault, "Transistor selection and design of a VHF dc-dc power converter," *IEEE Transactions on Power Electronics*, vol. 27, pp. 27–37, January Jan, 2008.

[14] R. Pilawa-Podgurski, A. Sagneri, J. Rivas, D. Anderson, and D. Perreault, "High-Frequency Resonant Boost Converters," in *IEEE Power Electronics Specialists Conference*, 2007.

[15] J. Kassakian, M. Schlecht, and G. Verghese, *Principles of Power Electronics*. NY: (Addison-Wesley), 1991.

[16] W. Everitt and G. Anner, *Communications Engineering*. New York: (McGraw-Hill), third ed., 1956.

[17] Y. Han and D. J. Perreault, "Analysis and design of high efficiency matching networks," *IEEE Transactions on Power Electronics*, vol. 21, pp. 1484–1491, September 2006.

[18] N. Sokal and A. Sokal, "Class E—a new class of high-efficiency tuned single-ended switching power amplifiers," *IEEE Journal of Solid-State Circuits*, vol. SC-10, no. 3, pp. 168–176, June 1975.

[19] N. O. Sokal, "Class-E RF Power Amplifiers," *QEX*, pp. 9–20, Jan/Feb 2001.

[20] M. J. Chudobiak, "The use of parasitic nonlinear capacitors in Class E amplifiers," *IEEE Transactions on Circuits and Systems I: Fundamental Theory and Applications*, vol. 41, pp. 941–944, December 1994.

[21] J. M. Rivas, Y. Han, O. Leitermann, A. D. Sagneri, and D. J. Perreault, "A high-frequency resonant inverter topology with low voltage stress," in *IEEE Power Electronics Specialist Conference*, 2007.

[22] J. M. Rivas, *Radio Frequency dc-dc Power Conversion*. Sc.D. Thesis, Dept. of Electrical Engineering and Computer Science, Massachusetts Institute of Technology, Cambridge, MA., September 2006.

[23] J. W. Phinney, D. J. Perreault, and J. H. Lang, "Radio-Frequency Inverters With Transmission-Line Input Networks," *IEEE Transactions on Power Electronics*, vol. 22, pp. 1154–1161, 2007.

[24] J. W. Phinney, D. J. Perreault, and J. H. Lang, "Synthesis of Lumped Transmission-Line Analogs," *IEEE Transactions on Power Electronics*, vol. 22, pp. 1531–1542, 2007.

[25] J. W. Phinney, *Multi-resonant Passive Components for Power Conversion*. Ph.D. Thesis, Dept. of Electrical Engineering and Computer Science, Massachusetts Institute of Technology, Cambridge, MA., June 2005.

[26] J. Rivas, *Radio Frequency dc-dc Power Conversion*. Ph.D. Thesis, Dept. of Electrical Engineering and Computer Science, Massachusetts Institute of Technology, Cambridge, MA, August 2006.

[27] I. Directed Energy, "Deic420 20 ampere low side ultrafast rf mosfet driver," Datasheet 9200-0230 Rev 3, IXYS RF, 2002.

[28] M. Iwadare and S. Mori, "Even harmonic resonant class E tuned power amplifer without RF choke," *Electronics and Communications in Japan, Part I*, vol. 79, no. 1, pp. 23–30, January 1996.